Cite this: *Dalton Trans.*, 2021, **50**,
2606

Stable supercapacitor electrode based on two-dimensional high nucleus silver nano-clusters as a green energy source†

Jing Zhuge,^{†a} Farzaneh Rouhani,^{†b} Fahime Bigdeli,^{†b} Xue-Mei Gao,^{†c}
Hamed Kaviani,^b Hong-Jing Li,^c Wei Wang,^c Mao-Lin Hu,^{†*a} Kuan-Guan Liu^{*c} and
Ali Morsali^{†*b}

Atomically precise silver nanoclusters (Ag-NCs) are known as a hot research area owing to their brilliant features and they have attracted an immense amount of research attention over the last year. There is a lack of sufficient understanding about the Ag-NC synthesis mechanisms that result in optimal silver nano-clusters with an appropriate size, shape, and morphology. In addition, the coexisting flexible coordination of silver ions, the argentophilic interactions, and coordination bonds result in a high level of sophistication in the self-assembly process. Furthermore, the expansion of clusters by the organic ligand to form a high dimensional structure could be very interesting and useful for novel applications in particular. In this study, a novel two-dimensional 14-nucleus silver poly-cluster was designed and synthesized by the combination of two synthetic methods. The high nucleus silver cluster units are connected together *via* tetradecafluoroazelaic acid (CF₂) and this leads to the high stability of the polymer. This highly stable conductive poly-cluster, with bridging groups of difluoromethylene, displays a high energy density (372 F g⁻¹ at 4.5 A g⁻¹), excellent cycling stability, and great capacity. This nanocluster shows a high power density and long cycle life over 6000 cycles (95%) and can also tolerate a wide range of scan rates (5 mV s⁻¹ to 1 V s⁻¹), meaning it could act as a green energy source.

Received 18th October 2020,
Accepted 18th January 2021

DOI: 10.1039/d0dt03608k

rsc.li/dalton

Introduction

The supramolecular assemblies of bridged molecular oxides, organic shells and metal ions lead to the formation of metal clusters.^{1,2} The connections of the metal ions to the organic shell, usually formed of organic ligands, determine the dimensions of the product and often prevent further polymerization.^{3,4} The properties of these nano-meter scale materials are different from those of their ingredients.^{5,6} In more precise terms, unlike the nanoparticles, clusters have a well-defined composition and identical structure, size and

form.^{7–9} The brilliant properties of the group 11 elements (Cu, Ag and Au), such as the enhanced metallophilic interactions, have led to their frequent use in the synthesis of novel cluster complexes to overcome repulsion between cationic metal centers. Among the nanoclusters of the group 11 elements, high-nuclearity Ag-NCs with atomically precise properties and diverse structures have attracted a tremendous amount of research interest.^{4,10–15} Their atomically precise structures and well-defined compositions could be helpful in understanding the structure–property relationships of the nanoclusters.^{6,16} Their attractive electronic and geometric features lead to promising physical/chemical performances in various fields of application, in particular catalysis, bio-sensing, and luminescence sensing processes.^{17,18}

The protecting ligands are highly effective in controlling the properties of silver NCs, and can control the size and structure of the product, and also play a vital role in dominant aggregation and stabilization of the clusters.^{19–23} In the structure of most Ag-NCs, the surface anchors include three kinds of conventional organic ligands and two types of inorganic ligands. Coexisting flexible coordination of the silver ions, argentophilic interactions and also a lack of understanding of the synthesis mechanism make studying the preparation of

^aCollege of Chemistry and Materials Engineering, Wenzhou University, Wenzhou 325035, China. E-mail: maolin_hu@yahoo.com

^bDepartment of Chemistry, Faculty of Sciences, Tarbiat Modares University, Tehran 14115-175, Iran. E-mail: Morsali_a@modares.ac.ir

^cState Key Laboratory of High-efficiency Coal Utilization and Green Chemical Engineering, and Ningxia Key Laboratory for Photovoltaic Materials, Ningxia University, Yin-Chuan, Ningxia, 750021, China. E-mail: liukuanguan@nxu.edu.cn

†Electronic supplementary information (ESI) available. CCDC 2020546. For ESI and crystallographic data in CIF or other electronic format see DOI: 10.1039/d0dt03608k

‡These authors contributed equally.

Ag-NCs with controlled features an attractive area.^{6,9,24,25} Therefore, establishing an accurate method to synthesize Ag-NCs with a controlled size and shape is highly desirable.

Generally, three typical synthesis methods based on temperature conditions are used for the formation of silver clusters: (i) low temperature, (ii) ambient temperature (which can be divided into stirring and ultra-sonication categories), and (iii) the solvothermal method.^{16,26}

Applying a series of changes in the structure of this type of material can be a method of engineering at the molecular level in order to access novel functional materials.^{27–29} Therefore, engineering and synthesis of the nano-polyclusters engender a wider range of potential applications.^{30,31} The cluster units of the polyclusters can be considered as constructing atoms of the molecules which are connected together by interaction between ligands or metals through metallophilic interactions to form high dimensional structures.³² For example, Au–Au interactions with proper orientations lead to the formation of a stable linear supracluster $\text{Au}_{25}(\text{SBu})_{18}$ in which the SBu ligand is butane thiolate.³³ In another example, $\text{Au}_{25}(\text{SCH}_2\text{CH}_2\text{CH}_3)_{18}$ clusters were formed through Au–SR motifs.³⁴ On the other hand, the formation of the polycluster structure resulted in metal–organic polyhedra (MOP) with widespread applications, which are strongly dependent on the coordination bonds, which connect the organic linkers together.^{35,36} To date, most of the synthesized networks of clusters include dimers or oligomers of the thiolated gold clusters and tetravalent actinides.^{37,38} Following on from these studies, we started to construct silver polyclusters by the combination of two synthetic methods (ambient temperature and solvothermal synthetic methods). In this study, a unique 14-nucleus silver poly-cluster based on a 2D polymer was prepared. In this structure, high nucleus cluster units connect together *via* tetradecafluoroazelaic acid (CF_2). The CF_2 sectors are rigid linear rods which adopt a helical configuration owing to intramolecular steric repulsions along the carbon backbone.

Porous carbon based materials are one of the most important composites for use in supercapacitors owing to their good electrical conductivity and large surface area. Porous carbons in combination with other elements, such as nitrogen, phosphorus and sulfur can improve the stability and performances of the supercapacitors.^{39,40} Recently, porous carbon materials obtained from natural materials such as PM2.5, pine needles and metal–organic frameworks were proposed as electrodes with a good performance for use in capacitors.^{41–43} Nano polyclusters provide an opportunity for the preparation of electrodes with a high performance and stability without any doping process or modification. Today, the significant impact of the presence of silver nanoparticles on the performance of supercapacitors is well known by researchers. Numerous groups have studied the significant effect of increasing the amount of Ag nanoparticles on the performance of all three types of supercapacitors.^{44–46} In the vast majority of reports, silver is used as an additive to the base structure to improve its properties, of which there are various examples.^{47–49} Direct use of silver thin film electrodes for supercapacitor applications was

reported by Oje *et al.*⁵⁰ A specific capacitance of 431 F g^{-1} at a 2 mV s^{-1} scan rate was achieved for the Ag thin film electrode produced at a 350 W forward power. However, no significant information was obtained about silver clusters to be used as supercapacitors. One of the vital factors that promotes the operation of supercapacitors is the electrical conductivity of the electrode active material. The extension of high nucleus coinage metal clusters in several dimensions can provide effective ways for electrons to pass through the structure and form a conductive poly-cluster.^{50,51}

In our previous study, we constructed an Ag_8 one-dimensional structure and used it as a supercapacitor electrode.³¹ The cyclic stability of the Ag_8 one-dimensional structure (SSc) is about 91% at 16 A g^{-1} for 5000 charge–discharge cycles. By changing the synthesis methods and outer ligands in that study, we attempted to achieve a high dimensional poly-cluster that could tolerate acidic or alkaline conditions for supercapacitive tests. Also, in high dimensional poly-clusters, the distance between the metallic nodes that were fixed by bridging ligands can affect the structural conductivity. In this study a facile method for the construction of a 14-nucleus two dimensional Ag poly-cluster is presented, by combination of the ambient and solvothermal methods. This conductive metallic 2D poly-cluster based on fluorinated derivatives of dicarboxylic acid is introduced as a supercapacitor electrode. Silver polyclusters without any modification process can act as a high performance stable electrode with a long cycle life over 6000 cycles (about 95%), an excellent power density and a high capacitance. The presence of fluorinated groups, the 2D expansion of the high nucleus metallic structure, and conductivity lead to form a effective supercapacitor electrode for green energy source.

2. Experimental

2.1. Materials and methods

The synthesis of the silver polyclusters $[\text{Ag}_{14}(\text{SPr}^{\dagger})_6(\text{C}_9\text{F}_{14}\text{O}_4)_4(\text{DMF})_8]_{\infty}$ (SPc) was performed by adding 0.132 g of tetradecafluoroazelaic acid (0.3 mmol) in a mixture of AgSPr^{\dagger} (0.055 g, 0.3 mmol) in 3 mL of DMF, AgTfa (tfa = trifluoroacetate, 0.066 g, 0.3 mmol) and AgOTf (OTf = trifluoromethanesulfonate, 0.077 g, 0.3 mmol) under 2 min of ultrasound treatment. The obtained colorless solution was mixed with 1 mL of a 0.1 M tetramethylammonium hydroxide in methanol. The achieved solution was sealed in a tube and heated to $70 \text{ }^\circ\text{C}$ overnight. After the reaction, the mixed solution was filtered, and the filtrate was evaporated at room temperature. Yield: 15.3 mg, 7.1% (based on AgSPr^{\dagger}). The crystal size used for the single crystal X-ray diffraction studies was $0.22 \times 0.18 \times 0.15 \text{ mm}$. The CCDC number of the SPc Structure is 2020546.†

2.2. Electrode preparation

A combination of the SPc acetylene black and polytetrafluoroethylene with 85 : 10 : 5 mass ratios was used for construction of the working electrode. The obtained viscous slurry was de-

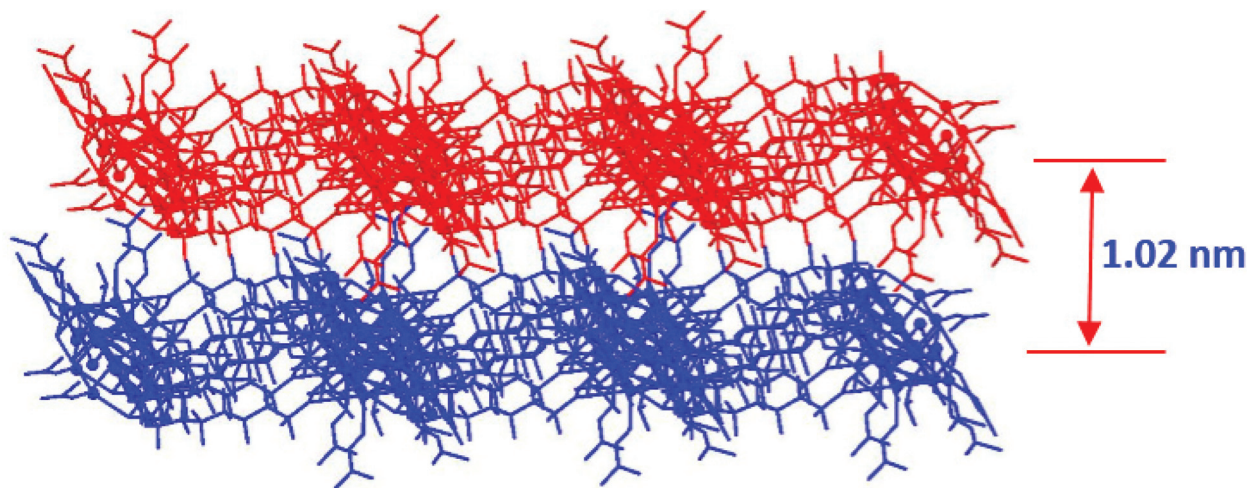


Fig. 2 Expansion of the 2D structure of SPc in the direction of $a \times c$.

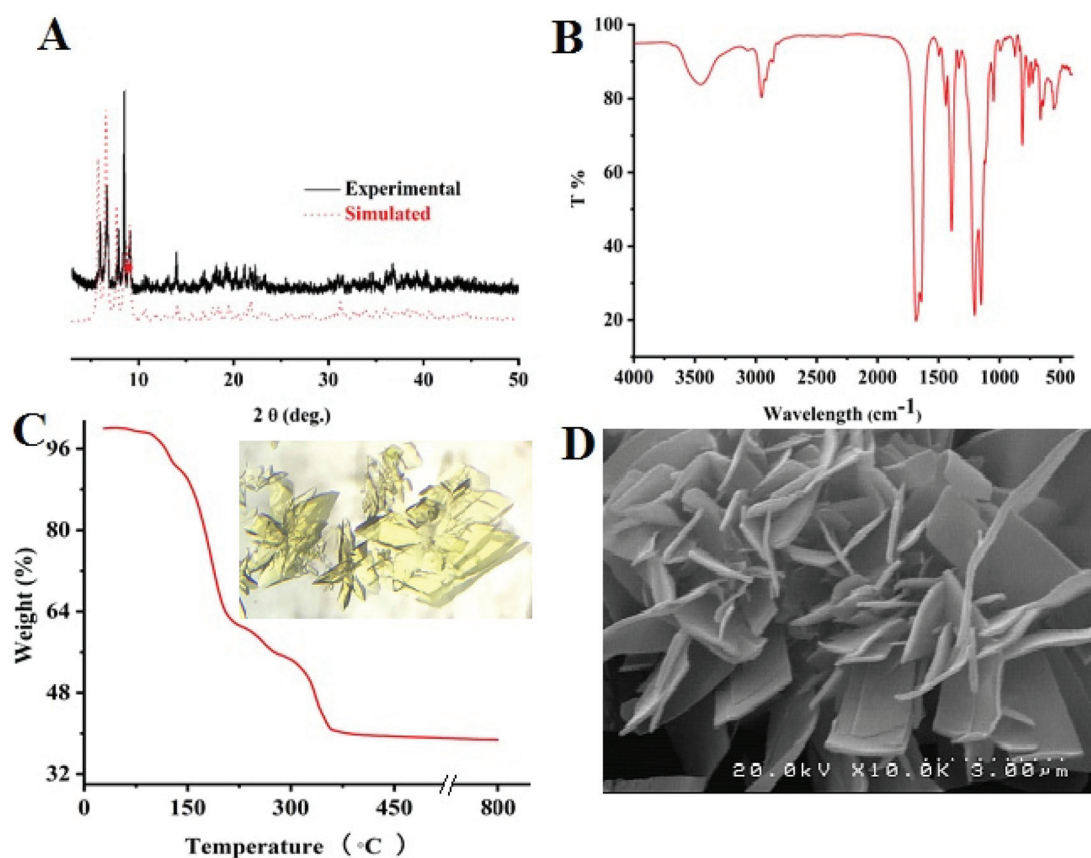


Fig. 3 (A) Comparison of the simulated XRD pattern and the experimental one, (B) the solid-state IR spectrum, (C) TGA spectrum (crystal picture inserted) and (D) SEM image of SPc.

the special morphology leads to better interaction of electrode material with electrolyte in favor of the occurrence of the redox process. The simultaneous presence of unique properties such as the presence of high nucleus silver clusters, expansion in two dimensions, special morphology, significant conductivity, and strong nature of Ag-S and C-F leads to the structural stabi-

lity, which led us to conduct supercapacitor studies using this structure.

A 2 M aqueous solution of potassium hydroxide was selected as the electrolyte. In order to study the stability of the structure, the SPc was immersed in the electrolyte (KOH, 2 M) for 4 h. The powder was separated by centrifugation and dried

at room temperature. The XRD pattern of the obtained sample and the simulated sample showed an acceptable match. Also, the inductively coupled plasma spectroscopy on the electrolyte shows a negligible amount of Ag ions (less than 2%) are released. This result confirms the stability of SPc in the selected electrolyte. The structural features, such as the strong metal–metal and Ag–S bonds, and the presence of the tetradecafluoroazelaic acid ligand can play an effective key role in the stability of SPc.

The SPc were used as a supercapacitor electrode in a three-electrode cell system. The CV (cyclic voltammetry) tests were performed in the 0 to +1 V potential range and at various scan rates from 50 to 1000 mV s^{-1} . The charge under the CV curve is due to the double-layer capacitance and the redox process at the electrode surface. The redox peaks within the 0.25 to 0.6 V potential range are mainly related to the faradaic silver oxidation states in the alkaline electrolyte (Fig. 4A).^{52,53} However, at higher scan rates (50–1000 mV s^{-1}) the faradaic peaks are buried under the very large double layer currents of the electrode (Fig. 4B). Furthermore, owing to the electrode internal resistance, the oxidation and reduction potentials were displaced in the positive and negative directions. Fig. 4C shows the CV curves obtained at a fixed scan rate (600 mV s^{-1}), but different applied voltages. The semi-rectangular shape of all the CV curves at different potential windows demonstrates the electric double layer features of the SPc. The high symmetry in the applied potential window confirms the significant electrochemical reversibility of the SPc.

The electrode charge storage mechanism for the charge storage system consists of two parts: the capacitance of the electric double layer and the diffusion-controlled contribution of the redox reaction of the electrochemically active material.⁵⁴ To determine the charge transfer kinetics of the SPc electrode, the power law was used to specify the contributions of the charge storage and diffusion-controlled reactions based on the CV results. The I_p shows that the peak current could be related to the scan rate (ν) based on eqn (1):

$$I_p = a\nu^b \quad (1)$$

In which, a and b are the adjustable parameters. The value of b is close to 0.5 or 1, if b is close to 0.5, the charge storage is primarily the result of a diffusion-controlled process, and if the b value is close to 1, the charge storage is the result of a capacitive process. The slope of $\log(i)$ versus $\log(\nu)$ plot, gives the b value (Fig. 5). The value of b obtained for the SPc electrode is 0.85, which indicates the dominance of the capacitive charge storage process in comparison with the diffusion-controlled process. Based on the various charge storage mechanisms of the CV behaviors at different scan rates, the contribution of the charge storage (capacitive and diffusion-controlled) can be separated. The charge storage contribution from the capacitive and diffusion-controlled processes can be separated based on the different charge storage mechanisms from the cyclic voltammetry behaviors at different scan rates. The currents from the electric double layer have a linear

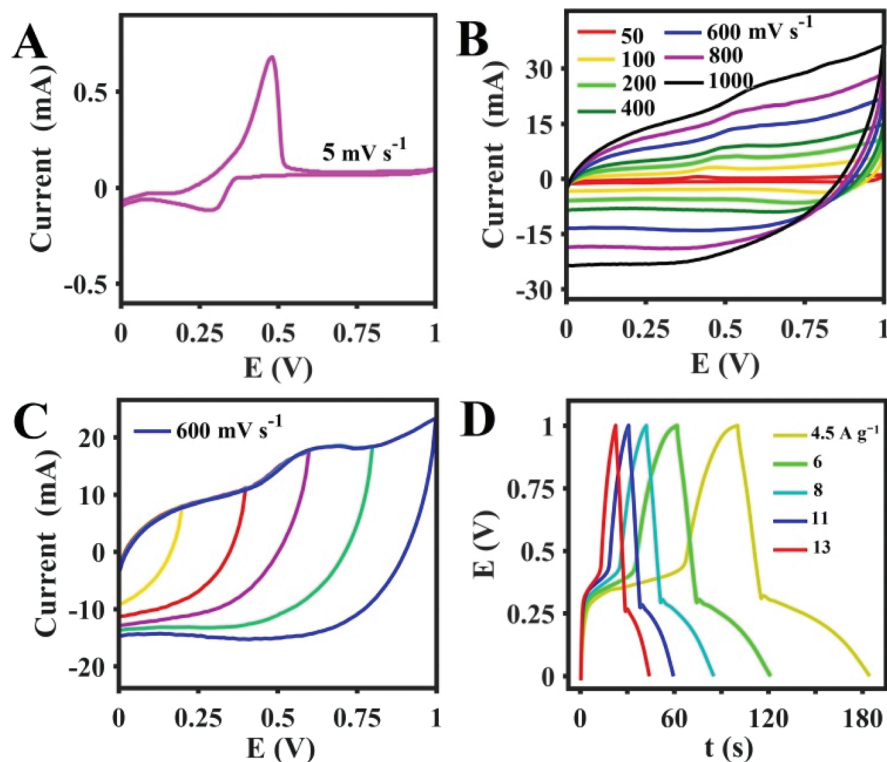


Fig. 4 (A) and (B) cyclic voltammetry curves of the SPc at low and high scan rates, respectively (C) CV at 600 mV s^{-1} and various call voltages, (D) GCD curves of the SPc at 4.5 to 13.0 A g^{-1} .

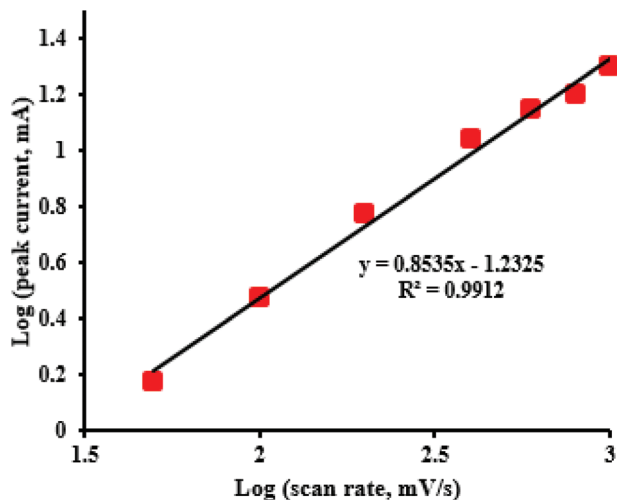


Fig. 5 Plot of $\log(i)$ versus $\log(v)$ for the SPc electrode.

relationship with the scan rates (v). The faradaic currents present a linear relationship with $v^{1/2}$. Thus, the total current at a specific potential can be divided into the following two parts: (eqn 2)

$$I_p = k_1 v + k_2 v^{1/2} \quad (2)$$

In which, I_p (A), k_1 and k_2 show the peak current and coefficients of the capacitive diffusion-controlled currents, respectively. This equation can also be changed to eqn (3), in which the amount of k_1 and k_2 achieved from the slope and intercept of the $I_p/v^{1/2}$ versus $v^{1/2}$ plot, respectively, can be represented as:

$$I_p/v^{1/2} = k_1 v^{1/2} + k_2 \quad (3)$$

Therefore, the contribution of the capacitance and diffusion-controlled current can be calculated separately, by inserting the values of k_1 and k_2 in eqn (3). The contributions at various scan rates are presented in Table S1.† The results

confirm that the dominant charge storage mechanism for the SPc electrode is a result of the capacitive process, rather than the diffusion-controlled process.

The obtained results of the galvanostatic charge/discharge curves (Fig. 4D) were used to calculate the specific capacitance (C_{sp}) based on eqn (1). The discharge current " I " (A), discharge time " Δt " (s), potential window during the time " ΔV " (V) and the mass of electrode " m " (g), were used for the calculation.

$$C_{sp} = (I \times \Delta t) / (\Delta V \times m) \quad (4)$$

The small kink in all the discharge curves is some kind of instrumental noise. The SPc provided the highest C_{sp} of 372 F g^{-1} at 4.5 A g^{-1} and the calculated C_{sp} at 6, 8, 11, and 13 A g^{-1} for SPc are 365, 360, 340, and 325 F g^{-1} , respectively. The first 30 charge/discharge curves for the SPc electrode at 11 A g^{-1} are presented in Fig. 6A. In addition, the cyclic stability of the poly-cluster was studied for 6000 cycles (11 A g^{-1} in a 0–1 V). As shown in Fig. 6B, 95% of the initial C_{sp} was maintained after 6000 cycles of charging and discharging, confirming the long cyclic stability of SPc as a supercapacitor electrode active material. In addition, the columbic efficiency of SPc at 4.5 A g^{-1} for 6000 cycles is about 97%, as presented in Fig. S3.†

Owing to the small size of the obtained crystals of SPc, which were unsuitable for direct conductivity measurements, the conductivity measurement was performed on a pressed pellet of SPc. The sheet electrical resistance values were measured using a conventional four probe measurement with the pellets (1 cm in diameter and 0.2 mm in thickness) at room temperature. The probes were in a straight line, the initial and final probes were used as a source of the current and the others were used to measure the voltage. As shown in Fig. S2,† a linear I - V curve was obtained. In addition, the conductivity of 2.3 S cm^{-1} was obtained for SPc. This measurement is not only beneficial for obtaining more accurate results, but also provides evidence of the electrical stability of the SPc.

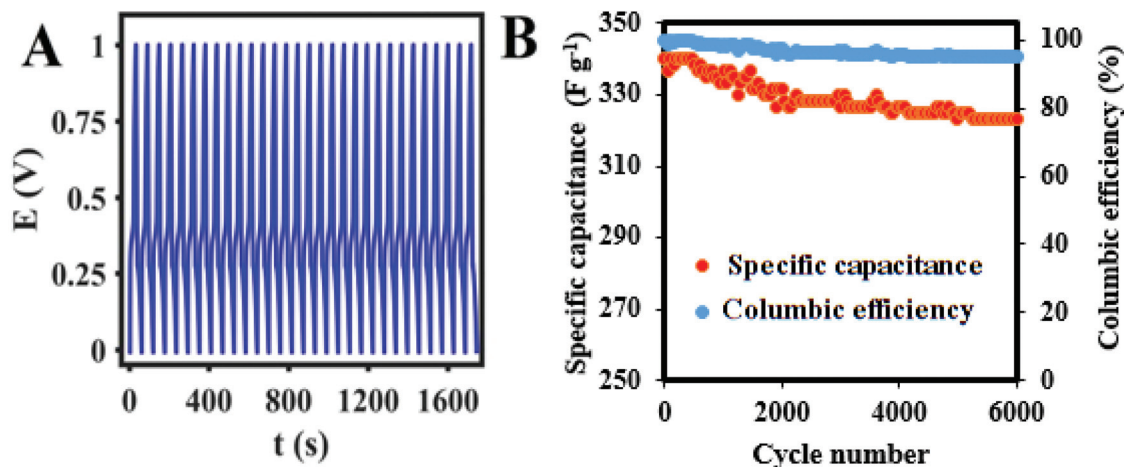


Fig. 6 (A) and (B) cycling stability and columbic efficiency of the SPc at 11 A g^{-1} for the first 30 and 6000 cycles.

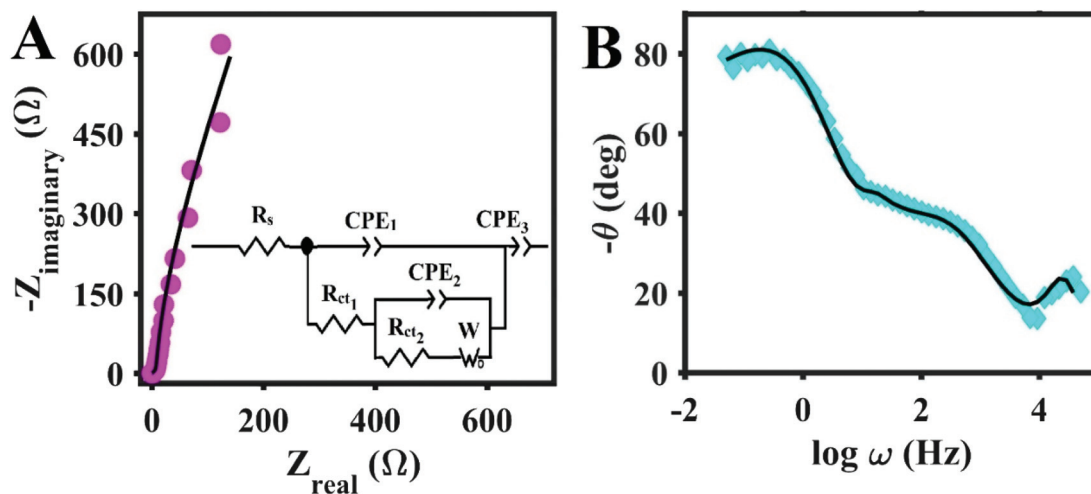


Fig. 7 (A) Nyquist plot (inset shows the corresponding electrical equivalent circuit), and (B) Bode-phase plot of the SPc.

On the other hand, the Nyquist and Bode plots, using electrochemical impedance spectroscopy (EIS) techniques (Fig. 7) were used to study the transport kinetics for the electrochemical behaviors of the SPc. The two interfacial charge transport processes occurred in the EIS-Nyquist plots of SPc which were confirmed by two semicircle trends (fitted in 50 kHz–50 mHz). The first one could be ascribed to the total charge transport resistance at the electrode/electrolyte interface (R_{ct1}), which is seen in the high-frequency region and the second semicircle (R_{ct2}) is ascribed to the total resistance of the charge transport at the interior interface of the SPc flakes.

Also, the tiny semicircles confirm the high speed ion diffusion to the electrode from the electrolyte.⁵⁵ In addition, the Warburg impedance (W) in the Nyquist plot of SPc is attributed to the diffusion of ions.⁵⁶ On the other hand, the changes in the phase angle with respect to the applied fre-

quency are displayed by the Bode-phase plot (Fig. 7B). The approximation of the phase angle to 80° indicates the ideal behavior of the SPc electrode as an appropriate active material for use as a supercapacitor electrode. Generally, the brilliant supercapacitive efficiency of SPc could be attributed to its appropriate morphology and good conductivity, which helps the electrons pass through the structure.

Furthermore, eqn (5) and (6) were used for calculation of the energy density, and power density, respectively:

$$E = (C \times V^2)/(2 \times 3.6) \quad (5)$$

$$P = (3600 \times E)/\Delta t. \quad (6)$$

The operating voltage window and discharge time is shown by the V (V) and Δt (s) symbols. The fabricated supercapacitor based on SPc in KOH (2 M) reveals values of 51.6 W h kg^{-1}

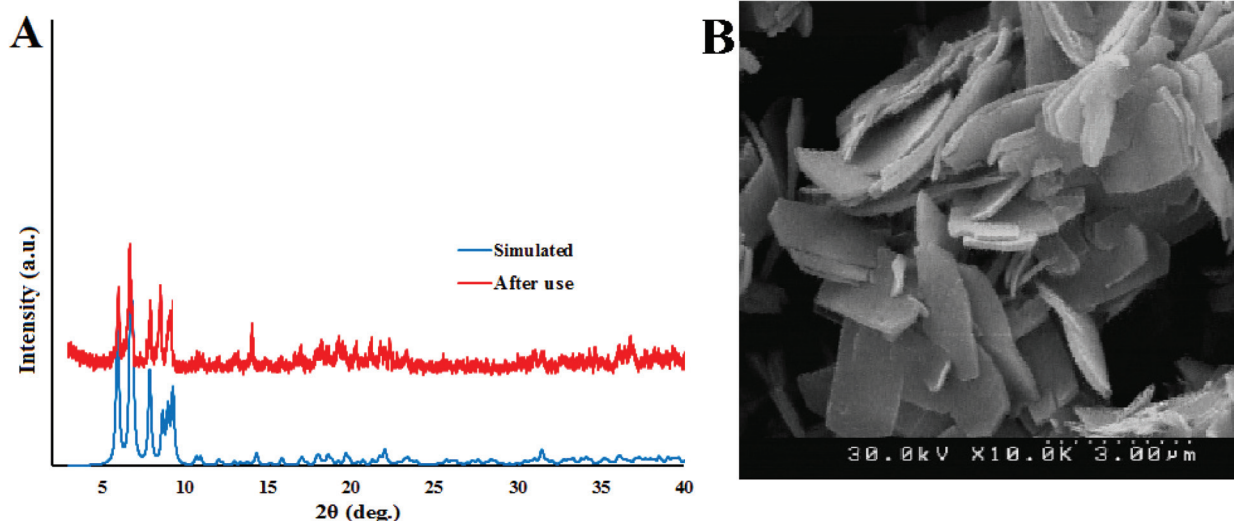


Fig. 8 (A) XRD pattern of SPc after 6000 charge/discharge cycles, (B) SEM images of SPc after use.

(energy density) and 2.32 kW kg^{-1} (power density). After use, the electrode materials were examined using SEM and powder XRD analysis. As shown in Fig. 8, the stability of the structure was confirmed by the intact XRD pattern. The stability of the structure could be related to the arrangement of the CF_2 groups on the superficial surface of SPc. The simultaneous operation of the double-layer and pseudo-capacitance performance of the silver nano-polymer and special features, such as the favorable morphology and low resistance of the structure, led to the remarkable supercapacitive efficiency of SPc. The simultaneous presence of these properties is very rare in non-hybrid materials.

4. Conclusion

In conclusion, for the first time, we synthesized silver polyclusters using a solvothermal method with the assistance of an ultrasonic technique. The tetradecafluoroazelaic acid acts as a bridging ligand to connect the cluster units to each other in the longitudinal and transverse directions. The function of these types of ligands is important in terms of both the structural architecture and the creation of potential applications, such as their use in supercapacitors. This conductive silver poly-cluster displays a faradaic capacitor behavior, 95% stability over 6000 cycles and higher specific capacitance in comparison with similar structures. The brilliant efficiency of these SPcs can be ascribed to the electronic conductivity and specific morphology of the active material. These features obliterate common obstacles such as low conductivity, multi-step synthesis, and agglomeration of the material. These results provide new horizons to expand the use of conductive metallic poly-clusters as a green energy source.

Conflicts of interest

There are no conflicts to declare.

Acknowledgements

This work was supported by the Natural Science Foundation of China (21571143 and 21601097), the Science & Technology Project for Young and Middle-aged Talents (Grant No. TJGC2018036), the Foundation of State Key Laboratory of High-efficiency Utilization of Coal and Green Chemical Engineering (Grant No. 2019-KF-01) and Tarbiat Modares University.

References

- 1 F. A. Cotton, Molybdenum compounds, in *Multiple Bonds Between Metal Atoms*, Springer, 2005, pp. 69–182.
- 2 K. Singh, M. Panghal, S. Kadyan and J. P. Yadav, Evaluation of antimicrobial activity of synthesized silver nanoparticles

- using *Phyllanthus amarus* and *Tinospora cordifolia* medicinal plants, *J. Nanomed. Nanotechnol.*, 2014, **5**, 1.
- 3 S. F. Yuan, C. Q. Xu, J. Li and Q. M. Wang, A Ligand-Protected Golden Fullerene: The Dipyritylamido Au_{328} +Nanocluster, *Angew. Chem.*, 2019, **131**, 5967–5970.
- 4 S.-S. Zhang, F. Alkan, H.-F. Su, C. M. Aikens, C.-H. Tung and D. Sun, $[\text{Ag}_{48}(\text{C}\equiv\text{C}^t\text{Bu})_{20}(\text{CrO}_4)_7]$: An Atomically Precise Silver Nanocluster Co-protected by Inorganic and Organic Ligands, *J. Am. Chem. Soc.*, 2019, **141**, 4460–4467.
- 5 D. Sun, Z.-H. Yan, V. A. Blatov, L. Wang and D.-F. Sun, Syntheses, topological structures, and photoluminescences of six new Zn(II) coordination polymers based on mixed tripodal imidazole ligand and varied polycarboxylates, *Cryst. Growth Des.*, 2013, **13**, 1277–1289.
- 6 Y.-P. Xie, J.-L. Jin, G.-X. Duan, X. Lu and T. C. Mak, High-nuclearity silver(I) chalcogenide clusters: a novel class of supramolecular assembly, *Coord. Chem. Rev.*, 2017, **331**, 54–72.
- 7 J. F. Corrigan, O. Fuhr and D. Fenske, Metal chalcogenide clusters on the border between molecules and materials, *Adv. Mater.*, 2009, **21**, 1867–1871.
- 8 C. P. Joshi, M. S. Bootharaju, M. J. Alhilaly and O. M. Bakr, $[\text{Ag}_{25}(\text{SR})_{18}]^-$: The “golden” silver nanoparticle, *J. Am. Chem. Soc.*, 2015, **137**, 11578–11581.
- 9 Z. Wang, H.-F. Su, Y.-Z. Tan, S. Schein, S.-C. Lin, W. Liu, S.-A. Wang, W.-G. Wang, C.-H. Tung and D. Sun, Assembly of silver Trigons into a buckyball-like Ag_{180} nanocage, *Proc. Natl. Acad. Sci. U. S. A.*, 2017, **114**, 12132–12137.
- 10 L. He, Z. Gan, N. Xia, L. Liao and Z. Wu, Alternating Array Stacking of Ag_{26}Au and Ag_{24}Au Nanoclusters, *Angew. Chem., Int. Ed.*, 2019, **58**, 9897–9901.
- 11 R. Jin, C. Zeng, M. Zhou and Y. Chen, Atomically precise colloidal metal nanoclusters and nanoparticles: fundamentals and opportunities, *Chem. Rev.*, 2016, **116**, 10346–10413.
- 12 E. Khatun, M. Bodiuzzaman, K. S. Sugi, P. Chakraborty, G. Paramasivam, W. A. Dar, T. Ahuja, S. Antharjanam and T. Pradeep, Confining an Ag_{10} Core in an Ag_{12} Shell: A Four-Electron Superatom with Enhanced Photoluminescence upon Crystallization, *ACS Nano*, 2019, **13**, 5753–5759.
- 13 J. W. Liu, Z. Wang, Y. M. Chai, M. Kurmoo, Q. Q. Zhao, X. P. Wang, C. H. Tung and D. Sun, Core Modulation of 70–Nuclei Core–Shell Silver Nanoclusters, *Angew. Chem.*, 2019, **131**, 6342–6345.
- 14 Z.-H. Pan, C.-L. Deng, Z. Wang, J.-Q. Lin, G.-G. Luo and D. Sun, Silver clusters templated by homo- and hetero-anions, *CrystEngComm*, 2020, **22**, 3736–3748.
- 15 Z. Wang, Y.-M. Sun, Q.-P. Qu, Y.-X. Liang, X.-P. Wang, Q.-Y. Liu, M. Kurmoo, H.-F. Su, C.-H. Tung and D. Sun, Enclosing classical polyoxometallates in silver nanoclusters, *Nanoscale*, 2019, **11**, 10927–10931.
- 16 Z. Wang, R. K. Gupta, G. G. Luo and D. Sun, Recent progress in inorganic anions templated silver nanoclusters: synthesis, structures and properties, *Chem. Rec.*, 2020, **20**, 389–402.

- 17 L.-P. Cheng, Z. Wang, Q.-Y. Wu, H.-F. Su, T. Peng, G.-G. Luo, Y.-A. Li, D. Sun and L.-S. Zheng, Small size yet big action: a simple sulfate anion templated a discrete 78-nuclearity silver sulfur nanocluster with a multishell structure, *Chem. Commun.*, 2018, **54**, 2361–2364.
- 18 Z. Wang, J.-W. Liu, H.-F. Su, Q.-Q. Zhao, M. Kurmoo, X.-P. Wang, C.-H. Tung, D. Sun and L.-S. Zheng, Chalcogens-Induced $\text{Ag}_6\text{Z}_4@ \text{Ag}_{36}$ (Z=S or Se) Core-Shell Nanoclusters: Enlarged Tetrahedral Core and Homochiral Crystallization, *J. Am. Chem. Soc.*, 2019, **141**, 17884–17890.
- 19 A. Schnepf and H. Schnöckel, Nanoscale Molecular Silver Cluster Compounds in Gram Quantities, *Angew. Chem., Int. Ed.*, 2014, **53**, 3064–3066.
- 20 G. G. Luo, H. F. Su, A. Xiao, Z. Wang, Y. Zhao, Q. Y. Wu, J. H. Wu, D. Sun and L. S. Zheng, Silver-Sulfur Hybrid Supertetrahedral Clusters: The Hitherto Missing Members in the Metal-Chalcogenide Tetrahedral Clusters, *Chem. - Eur. J.*, 2017, **23**, 14420–14424.
- 21 R. W. Huang, X. Y. Dong, B. J. Yan, X. S. Du, D. H. Wei, S. Q. Zang and T. C. Mak, Tandem silver cluster isomerism and mixed linkers to modulate the photoluminescence of cluster-assembled materials, *Angew. Chem., Int. Ed.*, 2018, **57**, 8560–8566.
- 22 S. Zhang and L. Zhao, Macrocyclic-encircled polynuclear metal clusters: controllable synthesis, reactivity studies, and applications, *Acc. Chem. Res.*, 2018, **51**, 2535–2545.
- 23 Z.-Y. Wang, M.-Q. Wang, Y.-L. Li, P. Luo, T.-T. Jia, R.-W. Huang, S.-Q. Zang and T. C. Mak, Atomically precise site-specific tailoring and directional assembly of superatomic silver nanoclusters, *J. Am. Chem. Soc.*, 2018, **140**, 1069–1076.
- 24 H. Yu, B. Rao, W. Jiang, S. Yang and M. Zhu, The photoluminescent metal nanoclusters with atomic precision, *Coord. Chem. Rev.*, 2019, **378**, 595–617.
- 25 H. Schmidbauer and A. Schier, Argentophilic interactions, *Angew. Chem., Int. Ed.*, 2015, **54**, 746–784.
- 26 G.-G. Luo, Q.-L. Guo, Z. Wang, C.-F. Sun, J.-Q. Lin and D. Sun, New protective ligands for atomically precise silver nanoclusters, *Dalton Trans.*, 2020, **49**, 5406–5415.
- 27 S. Mukherjee and P. S. Mukherjee, Versatility of azide in serendipitous assembly of copper(II) magnetic polyclusters, *Acc. Chem. Res.*, 2013, **46**, 2556–2566.
- 28 F. Rouhani, F. Rafizadeh-Masuleh and A. Morsali, Highly Electroconductive Metal-Organic Framework: Tunable by Metal Ion Sorption Quantity, *J. Am. Chem. Soc.*, 2019, **141**, 11173–11182.
- 29 F. Rouhani, F. Rafizadeh-Masuleh and A. Morsali, Selective sacrificial metal-organic frameworks: a highly quantitative colorimetric naked-eye detector for aluminum ions in aqueous solutions, *J. Mater. Chem. A*, 2019, **7**, 18634–18641.
- 30 K.-G. Liu, F. Rouhani, Q.-D. Shan, R. Wang, J. Li, M.-L. Hu, X. Cheng and A. Morsali, Ultrasonic-assisted fabrication of thin-film electrochemical detector of H_2O_2 based on ferrocene-functionalized silver cluster, *Ultrason. Sonochem.*, 2019, **56**, 305–312.
- 31 K.-G. Liu, F. Rouhani, H. Moghanni-Bavil-Olyaei, X.-W. Wei, X.-M. Gao, J.-Z. Li, X. Yan, M. L. Hu and A. Morsali, Conductive 1D High-nucleus Silver polymer as a Brilliant Non-hybrid Supercapacitor Electrode, *J. Mater. Chem. A*, 2020, **8**, 12975–12983.
- 32 R. Ho-Wu, K. Sun and T. Goodson III, Synthesis and enhanced linear and nonlinear optical properties of chromophore-au metal cluster oligomers, *J. Phys. Chem. C*, 2018, **122**, 2315–2329.
- 33 P. Chakraborty, A. Baksi, S. K. Mudedla, A. Nag, G. Paramasivam, V. Subramanian and T. Pradeep, Understanding proton capture and cation-induced dimerization of $[\text{Ag}_{29}(\text{BDT})_{12}]^{3-}$ clusters by ion mobility mass spectrometry, *Phys. Chem. Chem. Phys.*, 2018, **20**, 7593–7603.
- 34 M. Suyama, S. Takano, T. Nakamura and T. Tsukuda, Stoichiometric Formation of Open-Shell $[\text{PtAu}_{24}(\text{SC}_2\text{H}_4\text{Ph})_{18}]^{2-}$ via Spontaneous Electron Proportionation between $[\text{PtAu}_{24}(\text{SC}_2\text{H}_4\text{Ph})_{18}]^{2-}$ and $[\text{PtAu}_{24}(\text{SC}_2\text{H}_4\text{Ph})_{18}]^0$, *J. Am. Chem. Soc.*, 2019, **141**, 14048–14051.
- 35 X.-Y. Xie, F. Wu, X. Liu, W.-Q. Tao, Y. Jiang, X.-Q. Liu and L.-B. Sun, Photopolymerization of metal-organic polyhedra: an efficient approach to improve the hydrostability, dispersity, and processability, *Chem. Commun.*, 2019, **55**, 6177–6180.
- 36 M. Paul, N. Adarsh and P. Dastidar, Secondary Building Unit (SBU) Controlled Formation of a Catalytically Active Metal-Organic Polyhedron (MOP) Derived from a Flexible Tripodal Ligand, *Cryst. Growth Des.*, 2014, **14**, 1331–1337.
- 37 V. R. Jupally, R. Kota, E. V. Dornshuld, D. L. Mattern, G. S. Tschumper, D.-E. Jiang and A. Dass, Interstaple dithiol cross-linking in $\text{Au}_{25}(\text{SR})_{18}$ nanomolecules: a combined mass spectrometric and computational study, *J. Am. Chem. Soc.*, 2011, **133**, 20258–20266.
- 38 C. Falaise, C. Volkringer, J.-F. O. Vigier, A. Beaurain, P. Roussel, P. Rabu and T. Loiseau, Isolation of the Large {Actinide} 38 Poly-oxo Cluster with Uranium, *J. Am. Chem. Soc.*, 2013, **135**, 15678–15681.
- 39 G. Zhu, L. Ma, H. Lv, Y. Hu, T. Chen, R. Chen, J. Liang, X. Wang, Y. Wang, C. Yan, Z. Tie, Z. Jin and J. Liu, Pine needle-derived microporous nitrogen-doped carbon frameworks exhibit high performances in electrocatalytic hydrogen evolution reaction and supercapacitors, *Nanoscale*, 2017, **9**(3), 1237–1243.
- 40 G. Zhu, L. Ma, H. Lin, P. Zhao, L. Wang, Y. Hu, R. Chen, T. Chen, Y. Wang, Z. Tie and Z. Jin, High-performance Li-ion capacitor based on black- TiO_{2-x} /graphene aerogel anode and biomass-derived microporous carbon cathode, *Nano Res.*, 2019, **12**(7), 1713–1719.
- 41 G. Zhu, T. Chen, Y. Hu, L. Ma, R. Chen, H. Lv, Y. Wang, J. Liang, X. Li, C. Yan and H. Zhu, Recycling PM2.5 carbon nanoparticles generated by diesel vehicles for supercapacitors and oxygen reduction reaction, *Nano Energy*, 2017, **33**, 229–237.
- 42 H. Wang, Q. Yi, L. Gao, Y. Gao, T. Liu, Y. B. Jiang, Y. Sun and G. Zou, Hierarchically interconnected nitrogen-doped

- carbon nanosheets for an efficient hydrogen evolution reaction, *Nanoscale*, 2017, **9**(42), 16342–16348.
- 43 T. Liang, H. Wang, R. Fei, R. Wang, B. He, Y. Gong and C. Yan, A high-power lithium-ion hybrid capacitor based on a hollow N-doped carbon nanobox anode and its porous analogue cathode, *Nanoscale*, 2019, **11**(43), 20715–20724.
- 44 J. Stejskal and M. Trchová, Conducting polypyrrole nanotubes: a review, *Chem. Pap.*, 2018, **72**, 1563–1595.
- 45 X. Zhang, Q. Fu, H. Huang, L. Wei and X. Guo, Silver-quantum-dot-modified MoO₃ and MnO₂ paper-like free-standing films for flexible solid-state asymmetric supercapacitors, *Small*, 2019, **15**, 1805235.
- 46 T. Yeo, J. Lee, D. Shin, S. Park, H. Hwang and W. Choi, One-step fabrication of silver nanosphere-wetted carbon nanotube electrodes via electric-field-driven combustion waves for high-performance flexible supercapacitors, *J. Mater. Chem. A*, 2019, **7**, 9004–9018.
- 47 B. S. Singu and K. R. Yoon, Highly exfoliated GO-PPy-Ag ternary nanocomposite for electrochemical supercapacitor, *Electrochim. Acta*, 2018, **268**, 304–315.
- 48 L. Manjakkal, C. G. Núñez, W. Dang and R. Dahiya, Flexible self-charging supercapacitor based on graphene-Ag-3D graphene foam electrodes, *Nano Energy*, 2018, **51**, 604–612.
- 49 B. Pandit, V. S. Devika and B. R. Sankapal, Electroless-deposited Ag nanoparticles for highly stable energy-efficient electrochemical supercapacitor, *J. Alloys Compd.*, 2017, **726**, 1295–1303.
- 50 A. I. Oje, A. A. Ogwu, M. Mirzaeian, A. M. Oje and N. Tsendzughul, Silver thin film electrodes for supercapacitor application, *Appl. Surf. Sci.*, 2019, **488**, 142–150.
- 51 Q. Miao, F. Rouhani, H. Moghanni-Bavil-Olyaei, K.-G. Liu, X.-M. Gao, J.-Z. Li, X.-D. Hu, Z.-M. Jin, M.-L. Hu and A. Morsali, Comparative Study of the Supercapacitive Performance of three new Ferrocene-based Structures; Target Designed of a Conductive Ferrocene-Functionalized Coordination Polymer as supercapacitor electrode, *Chem. – Eur. J.*, 2020, **26**, 9518–9526.
- 52 P. Liu, J. Liu, S. Cheng, W. Cai, F. Yu, Y. Zhang, P. Wu and M. Liu, A high-performance electrode for supercapacitors: Silver nanoparticles grown on a porous perovskite-type material La_{0.7}Sr_{0.3}CoO_{3-δ} substrate, *Chem. Eng. J.*, 2017, **328**, 1–10.
- 53 S. Nagamuthu and K.-S. Ryu, Synthesis of Ag/NiO honeycomb structured nanoarrays as the electrode material for high performance asymmetric supercapacitor devices, *Sci. Rep.*, 2019, **9**, 1–11.
- 54 S. Liu, S. Sarwar, H. Zhang, Q. Guo, J. Luo and X. Zhang, One-step microwave-controlled synthesis of CoV₂O₆·2H₂O nanosheet for super long cycle-life battery-type supercapacitor, *Electrochim. Acta*, 2010, **364**, 137320.
- 55 J. Ji, X. Zhang, Z. Huang, X. Yu, H. Huang, Y. Huang and L. Li, One-step synthesis of graphene oxide/polypyrrole/MnO₂ ternary nanocomposites with an improved electrochemical capacitance, *J. Nanosci. Nanotechnol.*, 2017, **17**, 4356–4361.
- 56 J. Arjomandi, J. Y. Lee, R. Movafagh, H. Moghanni-Bavil-Olyaei and M. H. Parvin, Polyaniline/aluminum and iron oxide nanocomposites supercapacitor electrodes with high specific capacitance and surface area, *J. Electroanal. Chem.*, 2018, **810**, 100–108.